

Additive-Free, Aqueous CO₂ Hydrogenation with Ru/Polyphosphine-Based Solid Molecular Catalysts

Janine C. Baums,^[a] Isabella Kappel,^[b, c] Ansgar Meise,^[d] Marc Heggen,^[d] Claudia Weidenthaler,^[b] Peter J. C. Hausoul,^[a] and Regina Palkovits*^[a, c, e]

Molecular Ru complexes heterogenized on polyphosphine macroligands are identified as a highly active catalyst for the challenging direct hydrogenation of CO₂ in an aqueous environment. In DMSO/H₂O a TON of 2964 is reached and a high activity is retained in pure water (TON = 1500), due to the stabilizing effects of the polyphosphine on the reaction. The chemical

structure of the catalyst was elucidated through NMR, XPS, and PDF analysis. Comparison with the homogenous analog revealed that 44% of the activity is retained in the heterogeneous catalyst. The catalyst proved to be active over five hydrogen storage cycles, with no CO formation, and minor deactivation between 14–32%.

1. Introduction

In the search for a sustainable energy supply, H₂ from electrochemical water splitting is often discussed as a sustainable energy carrier.^[1] However, the transportation and storage of compressed H₂ presents challenges due to the increased weight and safety hazards of pressurized gas containers. In contrast, the hydrogenation of CO₂ gives liquid formic acid, which has a higher volumetric hydrogen density (53 g L⁻¹) than compressed H₂ at 700 bar and can be readily integrated into the existing gasoline infrastructure.^[2] Moreover, there is a growing market for formic acid itself, as it has broad applications in organic synthesis as a reducing agent and intermediate.^[3]

Currently, formic acid is synthesized from CO and water in a two-step process. Methanol is first carbonylated to methyl for-

mate, which is then hydrolyzed back to methanol and formic acid.^[4] It is estimated that the environmental impact of this process can be lowered by replacing the C1 source with sustainably derived CO₂ even when employing H₂ from a fossil source.^[5–7] Nevertheless, the direct hydrogenation of CO₂ is highly challenging, as CO₂ is both thermodynamically stable and kinetically inert. Even if the adverse entropy contribution is overcome by the dissolution of all reagents, the reaction has only a small negative Gibbs energy ($\Delta G^0 = -4 \text{ kJ mol}^{-1}$).^[8] By carrying the reaction out in the presence of a base (e.g., hydroxides, amines), reactivity is enhanced and the equilibrium shifted in favor ($\Delta G^0 = -35 \text{ kJ mol}^{-1}$) of formic acid formation. Under these conditions, CO₂ is available as carbonates (HCO₃⁻/CO₃²⁻) and converted to formate (HCO₂⁻).

Many homogeneous and heterogeneous catalytic systems effectively hydrogenate CO₂ under basic conditions.^[9–12] Highest activities and productivities were achieved with Ir and Ru PNP-pincer complexes (Ru TOF: 1,100,00 h⁻¹, Ir TON: 3,500,000).^[13,14] Among heterogeneous catalysts, single-atom catalysts show the most promising properties.^[15] Molecular Ru immobilized on a bipyridine-based porous organic polymer (POP) showed a high initial activity (38,800 h⁻¹).^[16] A modified Ru POP was used in a pilot scale trickle bed reactor for 30 days without noticeable deactivation, demonstrating the great potential of solid molecular systems (TON: 524,000).^[17] However, pure formic acid is only obtainable from the formate adduct through prior exchange of the amine, making the potential process unfeasible.^[18]

Aqueous FA solutions offer the additional advantage of being used as is in Direct Formic Acid Fuel Cells, which circumvents additional fugitive hydrogen emissions and additionally lowers the environmental impact.^[19] Still, the more challenging direct hydrogenation of CO₂ to formic acid under acidic conditions is only scarcely reported. Heterogeneous systems operating without additives in water are described, but only low conversions and thereby activities were reached (Pd/g-C₃N₄ TOF: 95 h⁻¹).^[20,21] The addition of basic groups on the catalyst surface can efficiently circumvent this by stabilizing formic acid and promoting its formation (Ru NPs on amine-functionalized

[a] J. C. Baums, Dr. P. J. C. Hausoul, Prof. Dr. R. Palkovits
Institut für Technische und Makromolekulare Chemie, RWTH Aachen
University, Worringerweg 2, Aachen 52074, Germany
E-mail: palkovits@itm.rwth-aachen.de
r.palkovits@fz-juelich.de

[b] Dr. I. Kappel, Prof. Dr. C. Weidenthaler
Max-Planck-Institut für Kohlenforschung, Kaiser-Wilhelm-Platz 1, Mülheim
an der Ruhr 45470, Germany

[c] Dr. I. Kappel, Prof. Dr. R. Palkovits
Institute for a Sustainable Hydrogen Economy, Forschungszentrum Jülich
GmbH, Marie-Curie-Str. 5, Jülich 52428, Germany

[d] A. Meise, Dr. M. Heggen
Ernst Ruska-Centrum für Mikroskopie und Spektroskopie mit Elektronen
(ER-C), Forschungszentrum Jülich GmbH, Wilhelm-Johnen-Straße, Jülich
52428, Germany

[e] Prof. Dr. R. Palkovits
Max-Planck-Institute for Chemical Energy Conversion, Stiftstr. 34-36,
Mülheim an der Ruhr 45470, Germany

Supporting information for this article is available on the WWW under
<https://doi.org/10.1002/cctc.202402048>

© 2025 The Author(s). ChemCatChem published by Wiley-VCH GmbH. This is
an open access article under the terms of the [Creative Commons Attribution](#)
License, which permits use, distribution and reproduction in any medium,
provided the original work is properly cited.

	Moret et al.	Rohmann et al.	this work
T, p, t	60 °C, 100 bar, 120 h	60 °C, 80 bar, 16 h	50 °C, 100 bar, 94 h
c(FA)	1.9 M	0.33 M	0.89 M
TON	179	4200	2990

Scheme 1. State of the art catalytic systems for CO₂ hydrogenation under acidic conditions.

SBA-15 TOF: 1289 h⁻¹).^[22,23] In a homogeneous catalyst system with [RuCl₂(PTA)₄] Moret et al. (Scheme 1) found that DMSO aids direct hydrogenation through solvent product interactions, reaching an unprecedented high FA concentration of 1.9 M in an acidic system, calculated to be the thermodynamic limit.^[24] With a Ru-PNP pincer complex by Rohmann et al. the activity in such a system was further improved.^[25]

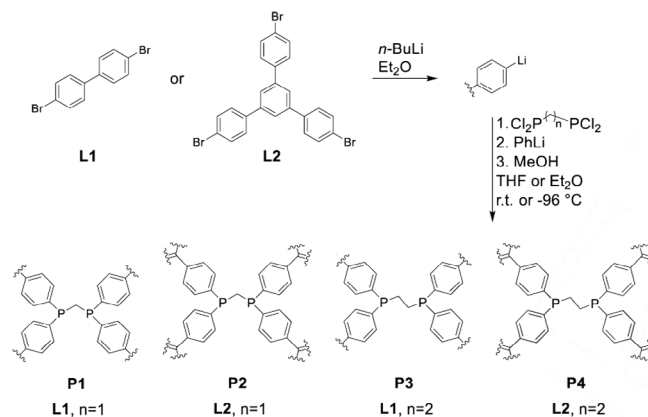
Heterogeneous, stable metal complexes can be obtained through macroligand structures. In the past, our group has presented molecular Ru immobilized on novel polyphosphines as catalysts.^[26] The system proved to be highly active in the hydrogenation of CO₂ to formate and methyl formate. Here, the established system is transferred to a base-free approach using a water/DMSO solvent system. The polymer synthesis is further developed, and the effect of the improved polymer on the acidic (de)hydrogenation studied. Finally, the potential of the catalytic system to perform under pure aqueous conditions is demonstrated and sequential hydrogenation and dehydrogenation is carried out.

2. Results and Discussion

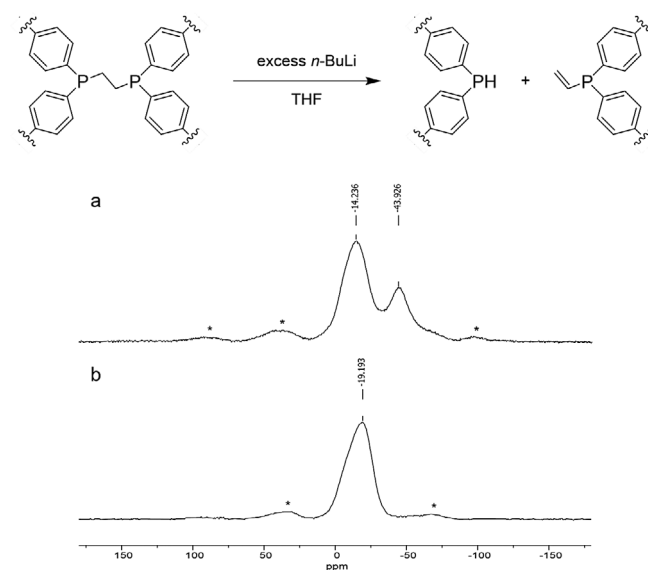
2.1. Polymer Synthesis

1,1-bis(diphenylphosphino)methane- (dppm) and 1,2-bis(diphenylphosphino)ethane-based (dppe) polyphosphines crosslinked with 4,4'-dibromobiphenyl (**L1**) or 1,3,5-tris(4-bromophenyl)benzene (**L2**) were prepared as described previously (Scheme 2).^[26–28] In brief, the linker is perlitiated with *n*-butyllithium (ⁿBuLi), filtered, and washed. Subsequently, the lithiated linker is cross-linked with a methyl- or ethyl-bridged bis(dichlorophosphine) and capped with phenyllithium to yield the polyphosphine polymers (**PN**_{T/S} (N = 1–4), T/S indicate the temperature and solvent employed in the crosslinking step). The chemical structure and purity of the polymers were characterized via solid-state ¹³C and ³¹P magic angle spinning (MAS) NMR.

For both dppm-based polymers **P1**_{rt/THF} and **P2**_{rt/THF}, a single resonance is observed in the ³¹P NMR spectra at –21.1 and –22.9 ppm, respectively. The ¹³C NMR spectra reveal broad signals corresponding to the aromatic (127.1–141.7 ppm) and bridging methylene (**P1**_{rt/THF} 25.3 ppm, **P2**_{rt/THF} 25.4 ppm) moiety. In addition, multiple sharper signals are observed in the aliphatic range (13.6–32.1 ppm) and at 65.2–70.2 ppm which stem from remain-



Scheme 2. Synthesis route of the tested polyphosphines.



Scheme 3. Proposed cleavage reaction of the dppe moiety leading to the formation of a secondary phosphine and a vinyl phosphine. Solid state MAS (10 kHz) ³¹P NMR of a cleaved **P3**_{rt/THF} (top) and **P3**_{rt/Et2O} (bottom) synthesized in Et₂O with a reduced amount of *n*-BuLi (spinning side bands are marked with an asterisk).

ing diethylether and *n*-pentane, which were used to wash the polymer after synthesis. For the ³¹P NMR of dppe-based polymer **P3**_{rt/THF}, a resonance at –14.8 ppm (dppe) and a large second resonance at –43.9 ppm are observed. It is proposed that the latter species is a secondary phosphine, resulting from an elimination reaction with co-precipitated ⁿBuLi as a nucleophile (Scheme 3). This is supported by a 2D ¹H-³¹P NMR which shows a strong resonance at 5 ppm and –44 ppm (Figure S13). By reducing the excess of ⁿBuLi and changing the solvent for the polymerization to Et₂O this could effectively be suppressed. In addition, it was tested to cool the polymerization step to –96 °C, which, by itself, is not sufficient to suppress the formation of the secondary phosphine completely. After adapting the synthesis route accordingly, a single phosphorous signal is obtained for **P3**_{rt/Et2O} (–15.0 ppm), **P4**_{rt/Et2O} (–19.1 ppm), and **P4**_{96/Et2O} (–19.0 ppm). As hereafter only polymers synthesized in Et₂O are discussed the solvent indices are omitted for legibility.

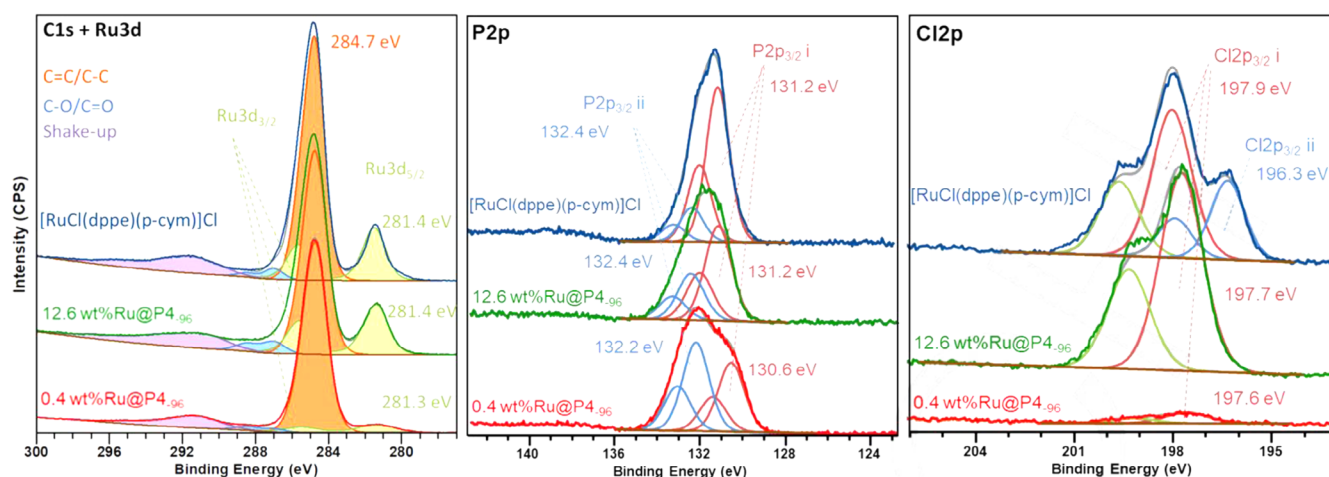


Figure 1. XPS high-resolution C 1s + Ru 3d (left), P 2p (middle) and Cl 2p (right) scans of 0.4 wt.% Ru@P_{4.96}, 12.6 wt.% Ru@P_{4.96} and [RuCl(dppe)(p-cymene)]Cl.

Nitrogen physisorption isotherms of the polymers were taken to determine specific surface area and micropore volume. Generally low surface areas of 3–197 m² g^{−1} are obtained. Polymers with a trifunctional linker polymerized at room temperature have the highest surface areas and are the only polymers with measurable micropore volume (0.022–0.056 mm³ g^{−1}). This is attributed to the higher amount of cross-linking in the structure. Comparing polymerization at room temperature and under cooling shows a significantly reduced surface area for the cooled polymers (Table S2).

Thermogravimetric analysis was used to characterize the polymers' thermal stability. All polymers showed stability up to 320 °C. Up to this temperature only a slight decrease (< 7.3%) in the mass ratio is observed, due to the desorption of residue solvent and gas (Figure S20). No further correlation between the used phosphine moieties, linkers, or synthesis method and the thermal stability of the resulting polymer is found.

2.2. Catalyst Preparation

Catalysts (Ru@PN_T, N = 1–4, T gives temperature during the crosslinking step) are obtained by immobilization of [Ru(p-cymene)Cl₂]₂ on the synthesized polyphosphines. ICP-MS revealed metal up-takes between 41–87% of the targeted 1 wt.% (Table S1). Survey XPS spectra of the synthesized P4 polymers show the presence of C, P, O, and F (Figure S16). The detected F is due to residual PTFE grease, which was used during polymer synthesis. The O signal is the result of residual solvent and previous handling of the samples under air. The P 2p spectrum shows the expected P^{III} spectrum with additional P^V, due to storing the samples under air prior to measurement (Figure 1). NMR previously confirmed the presence of only P^{III} of the polymer stored under inert gas, which was used for catalyst synthesis. The C 1s spectrum of the polymers confirms aromatic carbon to be the main carbon species. Analysis of the XPS survey scans of Ru@P_{4,t} and Ru@P_{4.96} after impregnation with [Ru(p-cymene)Cl₂]₂ show Ru and Cl photoelectron peaks,

further confirming the successful immobilization (Figure S17). The binding energies of the Cl 2p_{3/2} signal (197.5 and 197.7 eV) indicate that the Cl ligand is retained at the Ru center, confirming the targeted metal complex (Figure 1).^[29,30] The binding energy of both Ru 3d_{5/2} (281.2 and 281.4 eV) and 3p_{3/2} (462.4 eV) signals confirm Ru^{II} species.^[30] Also the absence of metallic Ru⁰ (Ru 3d: 279.9–280.1 eV)^[31–33] is noteworthy. However, the low metal loading in combination with an overlap of the C 1s and Ru 3d photoelectron peaks hinders in-depth analysis. An additional sample with 12.6 wt.% Ru@P_{4.96} was therefore prepared and shows one distinct Ru species (Ru 3d 281.3 eV) in good agreement with the 0.4 wt.% Ru@P_{4.96} catalyst (Δ = 0.1 eV). [RuCl(dppe)(p-cymene)]Cl as the expected structure was synthesized and measured as a reference. The binding energies of the immobilized species are in good agreement with the homogenous analog, confirming the successful identification of the immobilized metal complex. 12.6 wt.% Ru@P_{4.96} shows the P^{III} 2p signal (131.2 eV), shifted to a 0.7 eV higher binding energy compared to the unloaded polymer (Figure S18) due to the interaction with the metal sites. X-ray total scattering data of the dppe samples before and after impregnation with the Ru-precursor show no distinct Bragg reflections confirming a high dispersion of the metal and the amorphous nature of the support (Figure S19). With atomic pair distribution function (PDF) analysis based on the scattering data, interatomic distances within the aromatic ring (1.4, 2.4, 2.8 Å) are found, as well as an additional pair correlation at 1.8 Å, which stems from the P-C bonds (Figure 2). The assignment of the peaks is confirmed by comparison with the simulated PDF of dppe. As dppe is the shared building block between the polymers P_{3,rt}, P_{4,rt}, and P_{4.96}, the PDF peak positions remain as expected. The discrepancy in the peak intensities can be attributed to different carbon-to-phosphorous ratios resulting from the use of a smaller linker in P_{3,rt}. Difference PDF (dPDF) analysis allows the study of the changes in the material's local structure after impregnation with the Ru-precursor. The dPDF analysis between metal-free P_{4.96} and 0.4 and 12.6 wt.% Ru@P_{4.96} are shown in Figure 2. The simulated PDF of a reference structure (CCDC

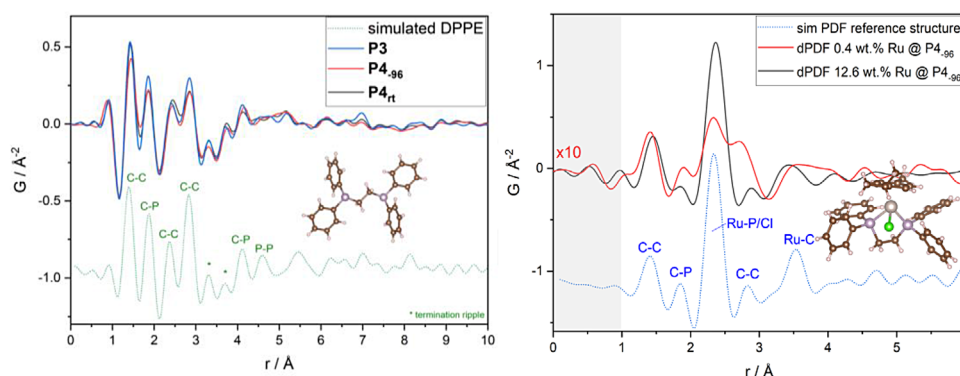


Figure 2. Pair distribution function analysis of the polymers (left) **P3_{rt}** (blue) **P4₉₆** (red) and **P4_{rt}** (grey) in comparison with the simulated PDF of DPPE (CCDC 2,065,417) and experimental difference PDFs (right) (dPDF = PDF(Ru@P4₉₆) – PDF(P4₉₆) – PDF(empty capillary)) of 0.4 wt.% (red, 10 x enlarged) and 12.6 wt.% (black) **Ru@P4₉₆** in comparison with a simulated PDF (blue) based on a molecular fragment of a reference structure [Ru(Cl)(dppe)(η -6-p-cymene)]BF₄ (CCDC RAHLIW).

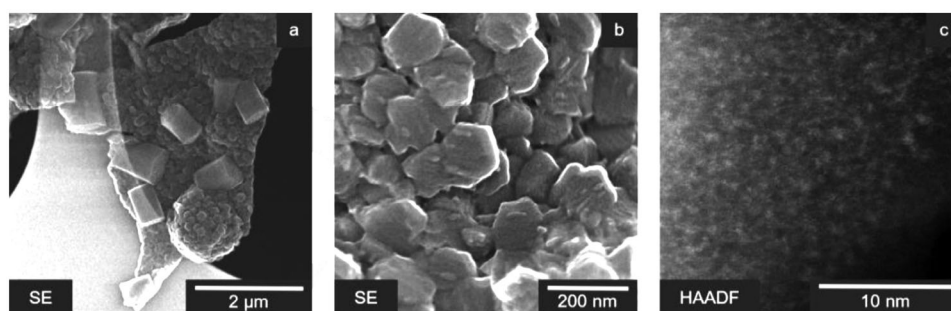


Figure 3. STEM imaging of pristine **Ru@P4_{rt}** catalyst (a, b, c) a, b: structure of polymer particles, c: structure of Ru immobilized on polymer.

refcode: RAHLIW), which is comparable with the proposed structure of this work as derived from XPS analysis, is plotted in comparison to the dPDFs. The pair correlations found in the PDF of the reference structure match with the pair correlations of the experimental dPDFs. The peak at 2.35 Å is in the range of Ru-P and Ru-Cl bonds reported in the literature and is especially dominant in the 12.6 wt.% **Ru@P4₉₆** sample.^[34,35] Furthermore, pair correlations at ~1.4 and 2.8 Å in the dPDFs confirm the presence of the p-cymene ligand after impregnation with the Ru-precursor. In further agreement with the XPS measurement, the interaction between the polyphosphine and metal and the proposed coordination environment of the complex is verified.

The catalyst **Ru@P4_{rt}** was further characterized by AC-STEM (Figure 3). In contrast to the expected amorphous structure, the polymer consists of larger rods (average length 620 nm) and smaller particles (average diameter 140 nm). Both resemble hexagonal shapes, which aligns with the symmetry of the trifunctional linker. SEM images of **Ru@P4_{rt}** and **Ru@P4₉₆** display similar rounded shapes, while **Ru@P3_{rt}** forms sharp platelets (Figures S21–S23). This further points towards the linker geometry causing the particle shape. Nevertheless, no lattice fringes are visible in agreement with XRD.

2.3. CO₂ Hydrogenation

CO₂ hydrogenation with the synthesized catalysts was tested (Table 1). All catalysts show activity in the hydrogenation reac-

Entry	Catalyst	Solvent	[FA] / M	TON
1	Ru@P1_{rt}	DMSO/H ₂ O	0.02	114
2	Ru@P1₉₆	DMSO/H ₂ O	0.08	332
3	Ru@P2_{rt}	DMSO/H ₂ O	0.06	245
4	Ru@P3_{rt}	DMSO/H ₂ O	0.35	1370
5	Ru@P4_{rt}	DMSO/H ₂ O	0.56	2769
6	Ru@P4₉₆	DMSO/H ₂ O	0.36	2966
7	Ru@P3_{rt}	H ₂ O	0.18	716
8	Ru@P4_{rt}	H ₂ O	0.16	807
9	Ru@P4₉₆	H ₂ O	0.18	1503

Conditions: 50 mL Hastelloy steel autoclaves, 30 mg catalyst, 3 μmol Ru, DMSO/ H₂O (9:1, v/ v, 10 mL), CO₂/ H₂ (1:1, p/ p, 100 bar), 50 °C, 94 h.

tion under acidic conditions. The lowest TONs of 114 (**Ru@P1_{rt}**) and 245 (**Ru@P2_{rt}**) are obtained with dpmm moieties. **Ru@P4₉₆** exhibits the highest activity with a TON of 2966. The highest FA concentration ([FA]) of 0.56 M is obtained with **Ru@P4_{rt}**. This shows that the dppe ligand structure is preferable for CO₂ hydrogenation, likely due to a more fitting bite angle and electronic properties.^[36] Regardless of the phosphine moiety, the trifunctional linker leads to catalysts with higher performance, which may also be attributed to the generally enhanced surface area of the polymers contributing to higher accessibility

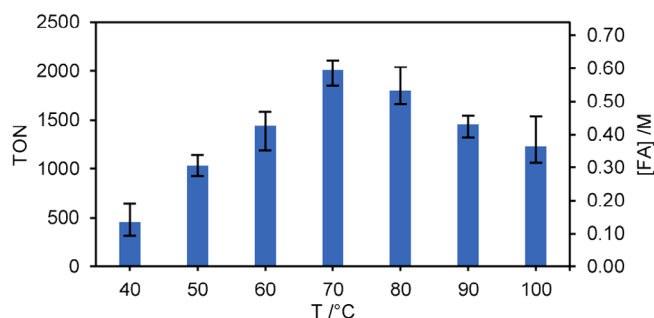


Figure 4. Temperature dependence of CO₂ hydrogenation with Ru@P4₉₆. Conditions: 50 mL Hastelloy steel autoclave, 10 mL DMSO/ H₂O (9:1, v/ v), 100 bar CO₂/ H₂ (1:1, p/ p), 30 mg catalyst, 3 μmol Ru, 18 h.

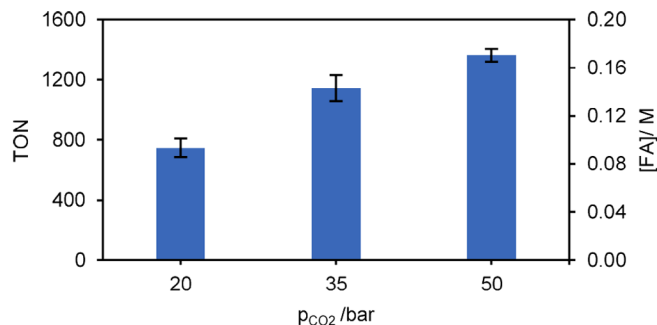


Figure 5. Obtained TON in the CO₂ hydrogenation with Ru@P4₉₆ at varied partial CO₂ pressures. Conditions: 50 mL Hastelloy steel autoclaves, 10 mL DMSO/ H₂O (9:1, v/ v), 100 bar CO₂/ H₂, 30 mg catalyst, 3 μmol Ru, 50 °C, 18 h.

of the reaction sites. However, between Ru@P1_{rt}, Ru@P1₉₆ and Ru@P4_{rt}, Ru@P4₉₆ the productivity increased by a factor of 2.9 and 1.1, respectively, showing that cooling the second synthetic step improves activity, despite a significantly lower surface area. The presence of phosphines in the polymers results in a slight basicity (pH 8.5 in water), which increases the concentration of CO₂ in the solution. This, in turn, facilitates the conversion of CO₂ to more reactive carbonates and stabilizes the product in the immediate vicinity of the catalytically active species. Therefore, DMSO to shift the reaction equilibrium can be omitted, to obtain an organic solvent-free reaction system, and the thereby obtained reaction solution has the potential to fuel direct formic acid fuel cells without further purification. The three best-performing catalysts Ru@P3_{rt}, Ru@P4_{rt}, and Ru@P4₉₆ were tested in pure water. All three catalysts retained a significant portion of their previous activity with the change of reaction system. Remarkably, Ru@P3_{rt} and Ru@P4₉₆ both show more than half of their productivity in the absence of DMSO. The attained concentrations (0.16–0.18 M) are considerably higher than the theoretical, thermodynamically limiting concentration of 0.1 M, thereby demonstrating a stabilizing influence of the macroligand on the reaction system.^[37]

The temperature dependence of the reaction was studied (Figure 4). The reaction time was shortened to 18 h for screening of the reaction parameters. The activity shows a maximum at 70 °C with a median TON of 2007 and a maximum FA concentration of 0.6 M. With a higher temperature the conversion rate increases as well as the solubility of hydrogen in DMSO/H₂O. Thereby, the highest TOF in this work of 111 h⁻¹ is obtained, which is slightly higher or in a similar order of magnitude to previously reported systems.^[20,21] However, heterogeneous, additive-free CO₂ hydrogenation is still scarcely reported, and the results are only comparable to a limited extent due to discrepancies in basicity and solvent. With further increasing temperature the equilibrium is shifted towards the reactants for this exergonic reaction, and the solubility of CO₂ diminishes, with 70 °C as a tradeoff between these factors. Therefore, the influence of the partial pressure of CO₂/H₂ was tested under a constant total pressure of 100 bar at 50 °C (Figure 5). The TON increases almost linearly with the partial pressure of CO₂. The simplest mechanism for CO₂ hydrogenation on single-atom catalysts is the CO₂ insertion into a metal hydride bond with the

Table 2. Comparison of immobilized catalyst and homogenous complex.

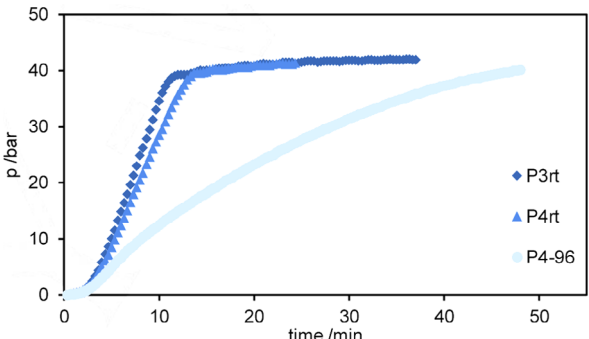
Entry	Catalyst	L/M	[FA] (M)	TON
1	Ru@P4 ₉₆	50	0.36	2964
2	Ru@P4 ₉₆ + P4 ₉₆	60	0.58	4725
3	[RuCl(dppe)(p-cymene)]Cl	1	0.04	1418
4	[RuCl(dppe)(p-cymene)]Cl + 49 eq. dppe	50	1.79	5998
5	[RuCl(dppe)(p-cymene)]Cl + 59 eq. dppe	60	2.90	9701

Conditions: 50 mL Hastelloy steel autoclaves, DMSO/ H₂O (9:1, v/ v, 10 mL), CO₂/ H₂ (1:1, p/ p 100 bar), 50 °C, 94 h. Polymer: 30 mg catalyst, 3 μmol Ru, [Ru(dppe)(p-cymene)]Cl: 3 μmol Ru.

following H₂ addition to regain the metal hydride species and yield formic acid.^[38] For Ru^{II} complexes, the latter is generally considered to be the rate-limiting step, although computational studies predict that both CO₂ and H₂ activation may be equally energetically favorable.^[39] The increasing activity of Ru@P4₉₆ with CO₂ availability through the increased pressure shows that CO₂ insertion is more crucial for this system than H₂ addition.

The influence of immobilization was investigated using [Ru(dppe)(p-cymene)]Cl as a homogeneous analog (Table 2). In a typical reaction with Ru@P4₉₆, the ligand-to-metal ratio (L/M) of 50 is comparably high and the polymeric network provides ample vacant coordination sites to help stabilize the coordinated Ru complex and prevent agglomeration. A first test was performed with the same amount of Ru-complex (L/M = 1, entry 3) as used in the heterogeneous reaction, yielding a TON of 1418.

When 49 eq. of dppe are added (L/M of 50) a TON of 5998 is obtained (entry 4). This is roughly double that of Ru@P4₉₆ (L/M = 50, TON 2964, entry 1). This shows that the immobilization does not have a strong adverse effect on the reaction. It should be noted, however, that dppe also acts as a base. As a result, more CO₂ dissolves, carbonates are formed, and the overall activity increases. This is further confirmed by entries 2 and 5, where the L/M was increased to 60, resulting in significantly higher TONs and FA concentrations.

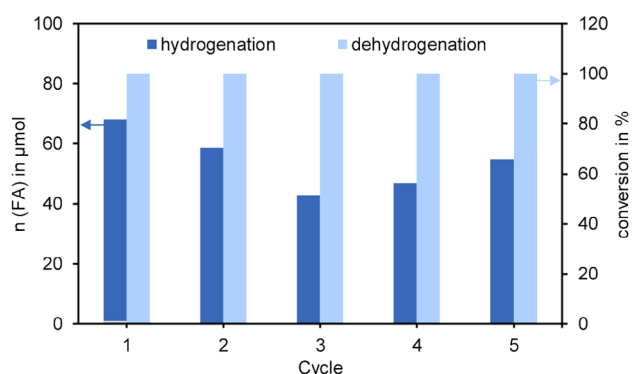
Table 3. Pressure curves and results of Ru@P3_{rt}, Ru@P4_{rt}, and Ru@P4₉₆ catalyzed formic acid dehydrogenation.


Entry	Catalyst	Conversion/ %	TOF _i /h ⁻¹	CO /ppm
1	Ru@P3 _{rt}	97.5	62,300	–
2	Ru@P4 _{rt}	95.6	51,000	–
3	Ru@P4 ₉₆	91.4	18,500	101

Conditions: 20 mL Hastelloy autoclave, 4 mL H₂O, 10 mmol formic acid, 12 mg catalyst, 1.2 μmol Ru, 160 °C, max. 45 min

2.4. Hydrogen Storage System

To investigate the potential of the catalysts in an organic solvent-free H₂ storage system, catalytic dehydrogenation of formic acid to CO₂ and H₂ was tested (Table 3). The three most active catalysts in the hydrogenation Ru@P3_{rt}, Ru@P4_{rt}, Ru@P4₉₆ were tested in the aqueous dehydrogenation. All show high conversions (>91%) and the initial TOFs were calculated from the linear segment of the pressure profile. Contrary to the hydrogenation, Ru@P3_{rt} is the most active catalyst and Ru@P4₉₆ shows the lowest activity. This is in line with our previous observations that under basic conditions hydrogenation and dehydrogenation follow different reaction pathways.^[26] It is most remarkable, that no CO was detected in the dehydrogenation with Ru@P3_{rt} and Ru@P4_{rt}. This renders these catalysts highly promising for use in a hydrogen storage system, given that CO is a poison for hydrogenation. Since Ru@P4_{rt} shows high activity in both reactions and no CO formation, it was further investigated using a series of hydrogenation and dehydrogenation reactions in water (Figure 6). After each hydrogenation and each dehydrogenation experiment, the gas phase and liquid phase were analyzed. The formic acid concentration and resulting pressure increase were insufficient to assess changes in the catalyst's dehydrogenation activity. Nevertheless, in all cases, dehydrogenation was complete and retained its high selectivity as no CO formation was detected. Remarkably, the catalyst remained active over five hydrogen storage cycles and exhibited a minor deactivation of 14%–37%. This finding contrasts our previous result that Ru@pDPPE undergoes rapid deactivation in three cycles during the amine-assisted CO₂ hydrogenation and FA dehydrogenation. This was attributed to the formation of CO during the dehydrogenation resulting in catalyst poisoning.^[26] In the current series, no CO formation was detected, which may explain the sustained activity of the catalyst. To assess changes in the active species

**Figure 6.** Results of consecutive CO₂ hydrogenation and FA dehydrogenation using Ru@P4_{rt}. Conditions: 20 mL Hastelloy steel autoclaves, 4 mL H₂O, 12 mg catalyst, 3 μmol Ru. Hydrogenation: 100 bar CO₂/H₂ (1:1, p/p), 50 °C, 18 h. Dehydrogenation: pressure released, atmosphere flushed with Ar, 160 °C, 30 min. During all reactions no CO formation was detectable.

during recycling and determine leaching, methodically identical hydrogen storage experiments were conducted with a 100 mg catalyst. After the last cycle, the Ru content in the solution is determined via ICP to be below 6 ppm, which corresponds to 25% of the metal immobilized in the catalyst. However, this is a considerable overestimation of the catalyst leaching, as the Ru content in the diluted samples is close to the lower detection limit.

The spent catalyst was characterized by AC-STEM imaging (Figure 7) and XPS (Figure 8). Imaging of the recycled catalysts shows no change in the polymer structure. The spent catalyst both after three and five hydrogen storage cycles shows nanoparticles. In contrast to the pristine catalyst, lattice fringes of the metallic regions are visible (Figure 7b). These are most likely formed under the harsher, reductive conditions of the dehydrogenation and future studies should therefore investigate lower temperatures in the decomposition. The nanoparticles are only present on a small fraction of the measured particles, which are depicted here (for additional images of the spent catalyst see Figure S24). On an exemplary image of the 3x recycled catalyst, 56 nanoparticles with a mean diameter of 6.0 nm were found (Figure 7a). In addition to particular species, the same single atom/clustered structures as on the pristine catalyst are found on the spent catalysts (Figure 7c). After five cycles only one large (Figure 7d, 20.7 × 11.8 nm) and three smaller (average diameter 2.6 nm) particles could be clearly identified and measured. As nanoparticles of Ru are inactive in the hydrogenation, the agglomeration is most likely causing the partial deactivation over multiple hydrogen storage cycles. It has been shown that Ru nanoparticles form CO in the catalytic formic acid dehydrogenation.^[40] Interestingly, no CO formation was observed despite the presence of nanoparticles, further pointing towards an overall small scale of nanoparticle formation.

In agreement with STEM imaging, XPS of the spent catalyst shows no indication of alteration of the polyphosphine framework during catalysis (Figure 8). In accordance, the NMR of the spent polymer affirms the stability of the polymer structure under reaction conditions (Figures S14 and S15). XPS of the spent

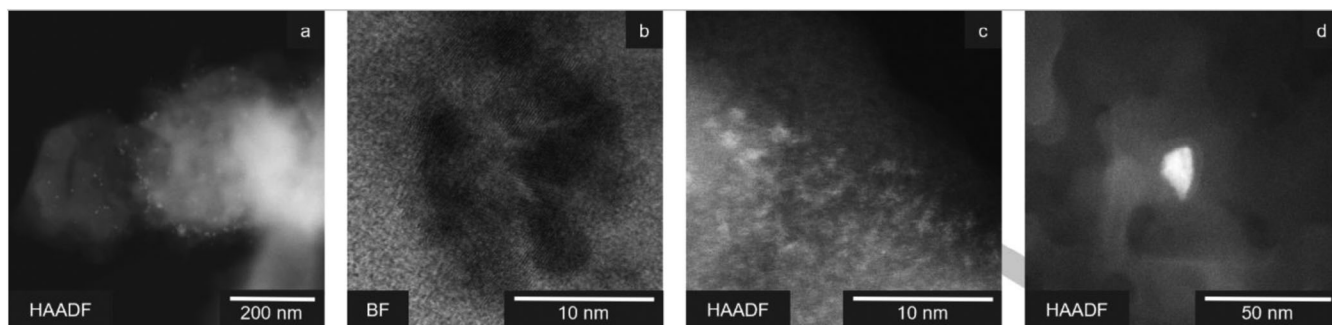


Figure 7. STEM imaging of spent Ru@P_{4rt} catalyst after three (a, b) and five (c, d) hydrogen storage cycles. (a and b) nanoparticles after three hydrogen storage cycles, (c) structure of Ru on polymer after five hydrogen storage cycles, and (d) nanoparticle after five hydrogen storage cycles.

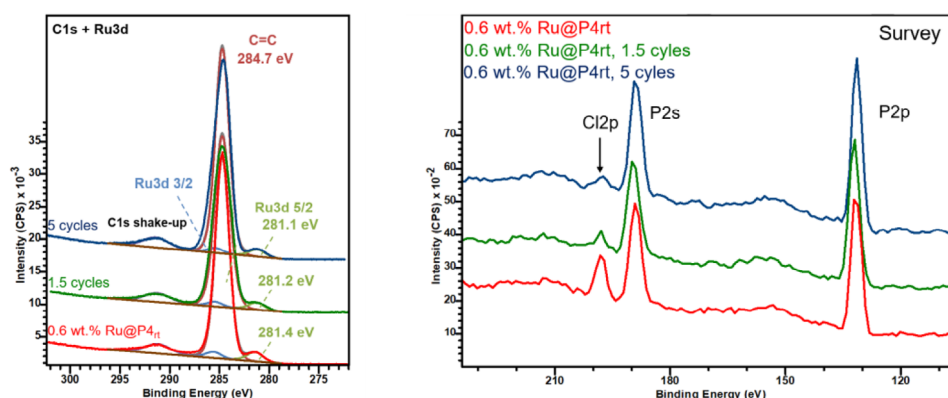


Figure 8. XPS C 1s + Ru 3d high resolution scans of 0.6 wt.% Ru@P_{4rt} pristine (red), 0.6 wt.% Ru@P_{4rt} after 1.5 cycles (green) and 0.6 wt.% Ru@P_{4rt} after 5 cycles (blue) (left). Zoom into the XPS survey scans of 0.6 wt.% Ru@P_{4rt} (red), 0.6 wt.% Ru@P_{4rt} after 1.5 cycles (green) and after 5 cycles (blue) (right). The decrease of the Cl 2p peak intensity indicates the loss of surface chlorine with increased catalytic cycles.

catalyst shows no sign of metallic Ru⁰. The Cl signal decreases significantly after the first two hydrogenations and then remains roughly constant over the five hydrogen storage cycles. The Cl bound to the Ru center is replaced by another X-type ligand, like formate or hydroxide, during the catalytic cycle. In accordance, the binding energy of the Ru 3d_{5/2} photoelectron peak decreases by 0.3 eV, further pointing towards a ligand exchange during the catalytic cycle. Additionally, a shift in the Ru 3d signal is found over the course of the recycling experiments, pointing towards a change in the coordination environment. As the metal's coordination mode defines its catalytic properties, this would contribute to the change in activity over the cycles.

3. Conclusion

The properties of solid molecular catalysts in CO₂ hydrogenation were investigated and a thereupon-based hydrogen storage system with exceptional selectivity and significantly improved stability was demonstrated. Through systematic variation of polymer synthesis, the ligand motif was found to be the main influence on the catalytic performance. In addition, changes in the structure of the polyphosphine through variations of the linker and polymerization temperature proved significant in shaping the reactivity. Differential PDF analysis revealed a Ru bond length of 2.35 Å, attributed to Ru-Cl and Ru-P bonds. The

structure of the catalyst was derived from XPS analysis, and a homogenous analog [RuCl(dppe)(p-cymene)]Cl was synthesized. The immobilized catalyst retained 44% of the activity of the homogenous analogue. It was found that the polyphosphine influences the reaction system, enabling high yields (0.19 M formic acid) in pure water and thereby an organic solvent-free H₂ storage system. The catalyst showed stable activity over 5 cycles with a decrease of 14%–37%. Minor nanoparticle formation was observed as a cause of deactivation in STEM. However, small-scale Ru structures, comparable to the pristine catalyst, prevail. Over all cycles, no CO formation was observed, which was the cause of fast deactivation in a previous system. This can be attributed to an adjusted synthesis route for the polymers. XPS analysis of the spent catalyst revealed the loss of the Cl[−] ligand over the catalytic cycle. Changes in the coordination environment also influence the activity, but for a clear understanding, further in-depth characterization to identify the active species is necessary. Otherwise, the coordination of the Ru center at the macroligand is retained.

Acknowledgements

This work was supported by the Kopernikus Project P2X-2: Flexible use of renewable resources – exploration, validation and implementation of “Power-to-X” concepts (03SF2A-2) funded

by the German Federal Ministry of Education and Research (BMBF) and by the Cluster of Excellence Fuel Science Center (EXC 2186, ID: 390919832) funded by the Excellence Initiative by the German federal and state governments to promote science and research at German universities. The authors acknowledge the funding by the German Federal Ministry of Education and Research (BMBF) and the Ministry of Economic Affairs, Industry, Climate Action and Energy of the State of North Rhine-Westphalia through the project HC-H2. A.M. and M.H. gratefully acknowledge funding by the Deutsche Forschungsgemeinschaft (DFG) within grant no. 441718867. We acknowledge the support of Hitachi High-Technologies. We gratefully thank Sera Aksoyog˘lu for her work in the laboratory and Keanu Birkelbach, Nils Kurig, and Sebastian Seidel for their valuable time for discussions. We thank Dr. C. Fares from MPI für Kohlenforschung for solid-state NMR measurements of the catalyst after usage.

Open access funding enabled and organized by Projekt DEAL.

Conflict of Interests

The authors declare no conflict of interest.

Data Availability Statement

The data that support the findings of this study are available from the corresponding author upon reasonable request.

Keywords: Carbon dioxide activation · Green chemistry · Hydrogenation · Solid molecular catalysts · X-ray photoelectron spectroscopy

- [1] N. P. Brandon, Z. Kurban, *Philos. Transact. A Math. Phys. Eng. Sci.* **2017**, 375, 20160400.
- [2] J. Eppinger, K.-W. Huang, *ACS Energy Lett.* **2017**, 2, 188–195.
- [3] M. Pérez-Fortes, J. C. Schöneberger, A. Boulamanti, G. Harrison, E. Tzimas, *Int. J. Hydrog. Energy* **2016**, 41, 16444–16462.
- [4] J. Hietala, A. Vuori, P. Johnsson, I. Pollari, W. Reutemann, H. Kieczka, in *Ullmann's Encyclopedia of Industrial Chemistry*, VCH, Weinheim, Germany **2016**, pp. 1–22.
- [5] A. Sternberg, C. M. Jens, A. Bardow, *Green Chem.* **2017**, 19, 2244–2259.
- [6] J. Mertens, C. Breyer, K. Arning, A. Bardow, R. Belmans, A. Dibenedetto, S. Erkman, J. Griepkoven, G. Léonard, S. Nizou, D. Pant, A. S. Reis-Machado, P. Styring, J. Vente, M. Webber, C. J. Sapart, *Joule* **2023**, 7, 442–449.
- [7] D. Kang, J. Byun, J. Han, *Green Chem.* **2021**, 23, 9470–9478.
- [8] P. G. Jessop, T. Ikariya, R. Noyori, *Chem. Rev.* **1995**, 95, 259–272.
- [9] K. Sordakis, C. Tang, L. K. Vogt, H. Junge, P. J. Dyson, M. Beller, G. Laurenczy, *Chem. Rev.* **2018**, 118, 372–433.
- [10] A. K. Singh, S. Singh, A. Kumar, *Catal. Sci. Technol.* **2016**, 6, 12–40.
- [11] A. Álvarez, A. Bansode, A. Urakawa, A. V. Bavykina, T. A. Wezendonk, M. Makkee, J. Gascon, F. Kapteijn, *Chem. Rev.* **2017**, 117, 9804–9838.
- [12] A. Modak, A. Ghosh, A. Bhaumik, B. Chowdhury, *Adv. Colloid Interface Sci.* **2021**, 290, 102349.
- [13] G. A. Filonenko, R. van Putten, E. N. Schulp, E. J. M. Hensen, E. A. Pidko, *ChemCatChem* **2014**, 6, 1526–1530.
- [14] R. Tanaka, M. Yamashita, K. Nozaki, *J. Am. Chem. Soc.* **2009**, 131, 14168–14169.
- [15] R. Sun, Y. Liao, S.-T. Bai, M. Zheng, C. Zhou, T. Zhang, B. F. Sels, *Energy Environ. Sci.* **2021**, 14, 1247–1285.
- [16] G. H. Gunasekar, K.-D. Jung, S. Yoon, *Inorg. Chem.* **2019**, 58, 3717–3723.
- [17] K. Park, G. H. Gunasekar, S.-H. Kim, H. Park, S. Kim, K. Park, K.-D. Jung, S. Yoon, *Green Chem.* **2020**, 22, 1639–1649.
- [18] D. Kim, J. Han, *Appl. Energy* **2020**, 264, 114711.
- [19] I. Dutta, R. K. Parsapur, S. Chatterjee, A. M. Hengne, D. Tan, K. Peramaiah, T. I. Solling, O. J. Nielsen, K.-W. Huang, *ACS Energy Lett.* **2023**, 8, 3251–3257.
- [20] S. Masuda, K. Mori, Y. Kuwahara, C. Louis, H. Yamashita, *Appl. Energy Mater.* **2020**, 3, 5847–5855.
- [21] C. Mondelli, B. Puértolas, M. Ackermann, Z. Chen, J. Pérez-Ramírez, *ChemSusChem* **2018**, 11, 2859–2869.
- [22] V. Srivastava, *Catal. Surv. Asia* **2021**, 25, 192–205.
- [23] K.-R. Oh, Y. Han, G.-Y. Cha, A. H. Valekar, M. Lee, S. E. Sivan, Y.-U. Kwon, Y. K. Hwang, *ACS Sustainable Chem. Eng.* **2021**, 9, 14051–14060.
- [24] S. Moret, P. J. Dyson, G. Laurenczy, *Nat. Commun.* **2014**, 5, 4017.
- [25] K. Rohmann, J. Kothe, M. W. Haenel, U. Englert, M. Hölscher, W. Leitner, *Angew. Chem., Int. Ed.* **2016**, 55, 8966–8969.
- [26] A. Kipshagen, J. C. Baums, H. Hartmann, A. Besmehn, P. J. C. Hausoul, R. Palkovits, *Catal. Sci. Technol.* **2022**, 12, 5649–5656.
- [27] P. J. C. Hausoul, C. Broicher, R. Vegliante, C. Göb, R. Palkovits, *Angew. Chem., Int. Ed.* **2016**, 55, 5597–5601.
- [28] A. Kann, H. Hartmann, A. Besmehn, P. J. C. Hausoul, R. Palkovits, *ChemSusChem* **2018**, 11, 1857–1865.
- [29] P. Kluson, P. Krystynik, P. Dytrych, L. Bartek, *React. Kinet. Mech. Catal.* **2016**, 119, 393–413.
- [30] E. J. Smoll Jr., X. Chen, L. M. Hall, L. D'Andrea, J. M. Slattery, T. K. Minton, *J. Phys. Chem. C* **2020**, 124, 382–397.
- [31] C. S. Huang, M. Houalla, D. M. Hercules, C. L. Kibby, L. Petrakis, *J. Phys. Chem.* **1989**, 93, 4540–4544.
- [32] C. J. Powell, *J. Electron. Spectrosc. Relat. Phenom.* **2012**, 185, 1–3.
- [33] R. Nyholm, N. Martensson, *J. Phys. C: Solid State Phys.* **1980**, 13, L279.
- [34] A. A. Adeniyi, P. A. Ajibade, *J. Chem.* **2016**, 2016, 1.
- [35] B. Dutta, E. Solari, S. Gauthier, R. Scopelliti, K. Severin, *Organometallics* **2007**, 26, 4791–4799.
- [36] L. F. Szczepura, J. Giambra, R. F. See, H. Lawson, T. S. Janik, A. J. Jircitano, M. R. Churchill, K. J. Takeuchi, *Inorg. Chim. Acta* **1995**, 239, 77–85.
- [37] C. M. Jens, M. Scott, B. Liebergesell, C. G. Westhues, P. Schäfer, G. Franciò, K. Leonhard, W. Leitner, A. Bardow, *Adv. Synth. Catal.* **2019**, 361, 307–316.
- [38] A. Weilhard, K. Salzmann, M. Navarro, J. Dupont, M. Albrecht, V. Sans, *J. Catal.* **2020**, 385, 1–9.
- [39] B. Mondal, F. Neese, S. Ye, *Inorg. Chem.* **2015**, 54, 7192–7198.
- [40] A. Belouqui Redondo, F. L. Morel, M. Ranocchiaro, J. A. van Bokhoven, *ACS Catal.* **2015**, 5, 7099–7103.

Manuscript received: December 12, 2024

Revised manuscript received: February 9, 2025

Accepted manuscript online: March 8, 2025

Version of record online: April 9, 2025